Revealing pH-Dependent Activities and Surface Instabilities for Ni-Based Electrocatalysts during the Oxygen Evolution Reaction

Chunzhen Yang, Maria Batuk, Quentin Jacquet, Gwenaëlle Rousse, Wei Yin, Leiting Zhang, Joke Hadermann, Artem Abakumov, Giannantonio Cibin, Alan Chadwick, et al.

Revealing pH-Dependent Activities and Surface Instabilities for Ni-Based Electrocatalysts during the Oxygen Evolution Reaction

Chunzhen Yang,[a] Maria Batuk,[b] Quentin Jacquet,[a] Gwenaëlle Rousse,[acd] Wei Yin,[a] Leiting Zhang,[a] Joke Hadermann,[b] Artem M. Abakumov,[e] Giannantonio Cibin,[f] Alan Chadwick,[g] Jean-Marie Tarascon,[acdh] and Alexis Grimaud[*acd]

[a] Chimie du Solide et de l'Energie, Collège de France, UMR 8260, 75231 Paris Cedex 05, France

[b] EMAT, University of Antwerp, Groenenborgerlaan 171, B-2020 Antwerp, Belgium

[c] Réseau sur le Stockage Electrochimique de l'Energie (RS2E), CNRS FR3459, 33 rue Saint Leu, 80039 Amiens Cedex, France

[d] Department of Chemistry, UPMC, 4 Place Jussieu, 75005 Paris, France

[e] Skoltech Center for Electrochemical Energy Storage, Skolkovo Institute of Science and Technology, Moscow 143026, Russia

[f] Diamond Light Source, Harwell Science and Innovation Campus, Didcot, Oxfordshire OX11 0DE, U.K.

[g] School of Physical Sciences, University of Kent, Canterbury, Kent CT2 7NH, U.K.

[h] ALISTORE-European Research Institute, FR CNRS 3104, 80039 Amiens, France

email: alexis.grimaud@college-de-france.fr

Abstract

Multiple electrochemical processes are involved at the catalyst/electrolyte interface during the oxygen evolution reaction (OER). With the purpose of elucidating the complexity of surface dynamics upon OER, we systematically studied two Ni-based crystalline oxides ($LaNiO_{3-\delta}$ and $La_2Li_{0.5}Ni_{0.5}O_4$) and compared them with the state-of-the-art Ni-Fe (oxy)hydroxide amorphous catalyst. Electrochemical measurements such as rotating ring disk electrode (RRDE) and electrochemical quartz microbalance microscopy (EQCM), coupled with a series of physical characterizations including transmission electron microscopy (TEM) and X-ray absorption spectroscopy (XAS) are conducted to unravel the exact pH effect on both the OER activity and the catalyst stability. We demonstrate that for Ni-based crystalline catalysts the rate for surface degradation depends on the pH and is greater than the rate for surface reconstruction. This behavior is unlike for amorphous Ni oxyhydroxide catalyst which is found more stable and pH independent.

TOC

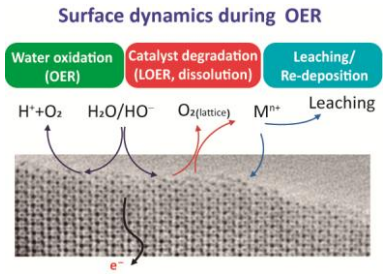

Water splitting is considered as a promising strategy to store energy from renewable energies in the form of a fuel (H_2) and has therefore attracted tremendous attention in recent years. [1-2] Nevertheless, the sluggish kinetics of the half reaction occurring at the anode, namely the oxygen evolution reaction (OER), currently limits the efficiency of the overall process, hence calling for the development of better electrocatalysts. Despite recent successes at designing earth-abundant crystalline or amorphous transitional metal oxides and oxyhydroxides,[3-6] our understanding of the active catalysts' structure and structural stability is still insufficient.

The activity of lattice oxygen for participating the in the OER has previously been investigated by isotopic labeling experiments coupled with differential electrochemical mass spectroscopy (DEMS) on RuO_2[7] and on Au electrode[8]. Results showed that O-O bonds could be formed between the lattice oxygen and surface absorbed oxygen, following a mechanism which can be compared to the well-known Mars-Van Krevelen (MvK) mechanism previously described for gas phase catalysis.[9] Recent discoveries further pointed towards common intermediates responsible for the involvement of lattice oxygen into the OER mechanism[7-8] but also into the surface degradation.[6, 10-13] Moreover, triggering the redox activity of lattice oxygen was found to often be associated with a strong pH dependence for the anodic current,[14-17] suggesting either a decoupled proton-electron-transfer mechanism for which the rate-determining step is shifting from the formation of O-O bonds to the deprotonation of $OH_{(ads)}$ or $OOH_{(ads)}$, or the chemical formation of pre-catalyst as being rate limiting. In any case, it was further demonstrated that the proton transfer kinetics at the catalyst/electrolyte interface becomes limiting for a wide variety of OER catalysts.[18-19] However, when the kinetics for refilling oxygen vacancies is slow, instability for oxide catalysts is often observed.[3, 20-21] This instability originates from cation dissolution which is triggered by the lowering of their coordination, hence often resulting in a rapid surface amorphization accompanied with a change of the

oxidation state for the transition metal on the surface, which led researchers to term these catalysts as redox active.[22-23] From these recent findings, understanding the delicate equilibriums existing on the surface of crystalline transition metal oxides appears to be vital for the development of efficient and stable OER catalysts. This is particularly true following recent knowledge developed for electrodeposited catalysts such as Co phosphate (CoP_i)[24-25] or Ni-Fe oxyhydroxide ($Ni_{1-x}Fe_xOOH$)[17, 26] for which a constant dissolution/redeposition process involved in the OER, also often poised as self-healing mechanism, places them at the border between solid heterogeneous and molecular homogenous catalysts.

In detail, the rapid surface reconstruction occurring for some oxide catalysts during the OER may involve multiple steps, including water adsorption and oxidation followed by oxygen release[27], catalyst degradation and cation dissolution induced by the evolution of lattice oxygen, the subsequent re-deposition process and the formation of amorphous surface with a structure often resembling that of (oxy)hydroxide-like species. So far, the complexity of the surface dynamics and our poor knowledge of the kinetics associated with each step hampered our understanding of the OER mechanism[28], hence calling for a protocol to accurately study these catalysts. This is especially true regarding the exact effect of pH which, by modifying the different equilibriums occurring at the catalyst/electrolyte interface, can impact both the activity and the stability of the catalysts. [17]

With the purpose of unveiling the pH effect on the underlying OER mechanism, we developed a redox active OER catalyst $La_2Li_{0.5}Ni_{0.5}O_{4\pm\delta}$ (LLNO) with Ruddlesden-Popper (RP) structure in which Li^+ serves as sacrificial cation that leaches out under OER conditions to activate the redox activity of the surface and initiate further surface degradation that we aim at studying in this work. This RP-type LLNO phase was designed as a redox active Ni^{3+} counterpart to $LaNiO_{3-\delta}$ which was

previously suggested to undergo lattice oxygen oxidation and evolution.[21] We then systematically studied the physical and electrochemical properties of these two Ni-based crystalline oxides and compared them with the state-of-the-art Ni-Fe (oxy)hydroxide ($Ni_{1-x}Fe_xOOH$) amorphous catalyst[26, 29] (Supplementary Figure S1). Coupling electrochemical tools such as rotating ring disk electrode (RRDE)[30-31] and electrochemical quartz microbalance microscopy (EQCM) with physical characterizations such as X-ray diffraction (XRD), transmission electron microscopy (TEM), and X-ray absorption spectroscopy (XAS) at Ni K-edge, we discuss in this study the exact effect of pH on both the OER activity and the catalyst stability for each of these different classes of compounds.

The structures of LLNO and $LaNiO_{3-\delta}$ were first examined using Rietveld refinements of data from laboratory XRD measurements (Figure 1a and Figure S1). The LLNO compound shows the Ruddlesden-Popper structure with a space group of I4/mmm, indicative of a disordering of NiO_6 and LiO_6 octahedra sharing corners and forming layers along the *ab* plane in between which La^{3+} cations occupy a position with 9-fold coordination.[32] $LaNiO_{3-\delta}$ possesses the rhombohedral perovskite structure with 3D arrangement of corner-shared NiO_6 octahedra. In contrary, the amorphous and electrodeposited Ni (oxy)hydroxide is composed of units of less than 10 edge-shared NiO_6 octahedra with terminal under-coordinated oxygen, as previously refined by XAS measurements.[29, 33-34]

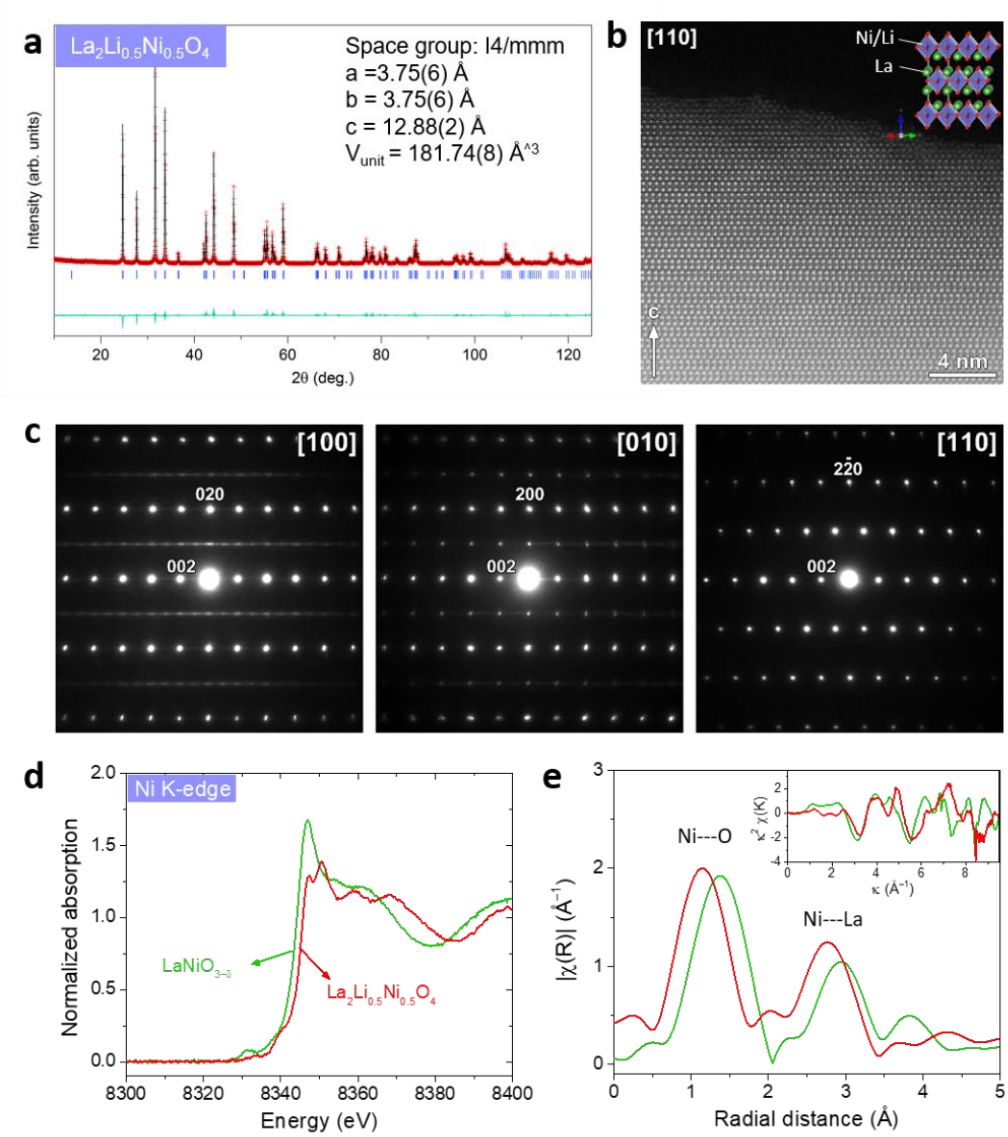

Figure 1. Structural characterizations of $La_2Li_{0.5}Ni_{0.5}O_4$. (a) X-ray powder diffraction pattern with Rietveld refinement. (b) [110] high-resolution HAADF-STEM image showing the structure of $La_2Li_{0.5}Ni_{0.5}O_4$. (c) Electron diffraction patterns along [100], [010], and [110] directions for $La_2Li_{0.5}Ni_{0.5}O_4$. (d) Ni K-edge XANES absorption spectra recorded for $La_2Li_{0.5}Ni_{0.5}O_4$ and $LaNiO_{3-\delta}$. (e) Magnitude of Fourier transform of K^3-weighted EXAFS oscillations for the pristine $La_2Li_{0.5}Ni_{0.5}O_4$ and $LaNiO_{3-\delta}$. In inset is shown the EXAFS oscillations in *k*-space.

Following this structural determination, the Ni oxidation state for crystalline LLNO and $LaNiO_{3-\delta}$ was determined by the means of Ni K-edge XAS spectroscopy (Figure

1d-e). When compared to $LaNiO_{3-\delta}$, a slight shift towards higher energy for the Ni K-edge was measured for LLNO, suggesting a slightly higher Ni oxidation state which could be explained by the presence of oxygen vacancies in $LaNiO_{3-\delta}$, as often reported for as synthetized compound.[35] The crystal structure of LLNO was further confirmed by TEM: high-angle annular dark-field scanning transmission electron microscopy (HAADF-STEM) images visualize the cations arrangement in the LLNO structure (Figures 1b, S2 and S3) and show a clean surface with only a very thin amorphous layer of 0.5 nm. Furthermore, while laboratory XRD was showing an average disordering of Li and Ni, electron diffraction patterns (Figure 1c) shows crystallites with a local ordering of NiO_6 and LiO_6 octahedra, confirming the *Ammm* symmetry and lattice parameters previously proposed. Finally, the 0kl: k+l=2n+1 reflections in the [100] patterns are due to twinning with [010].

Figure S4-S5 shows the electrochemical activity under OER conditions normalized by surface area as deduced by Brunauer, Emmet, Teller (BET) measurements for LLNO and $LaNiO_{3-\delta}$ and compared to the one measured for the nickel (oxy)hydroxide film as normalized by geometric surface area. Similar anodic currents as well as Tafel slopes were obtained for LLNO and $LaNiO_{3-\delta}$ after the first cycle, suggesting similar OER mechanism and kinetics for these two crystalline Ni-based compounds.

RRDE measurements[30-31] were further carried out to better understand the effect of pH on the anodic current, and more specifically the current resulting from the oxygen evolution on the surface of the catalyst from the contribution arising from catalyst degradation (Figure 2 and Figure S6). By calculating the collection efficiency $\eta = (i_{ring}/i_{disc})$ at a fixed potential (E = 1.6 V vs. RHE) at which the oxygen evolution occurs, the effective current contributing from oxygen evolution can thus be estimated.[30] The RRDE study reveals that the OER activity for both LLNO and $LaNiO_{3-\delta}$ increases with the pH while it remains mostly constant for the amorphous

film (Figure 2c). The collection efficiency for both LLNO and $LaNiO_{3-\delta}$ was found to decrease with pH from around 10% at pH 12.5 to around 5% at pH 14 (Figure 2e). In contrast, while the collection efficiency was also found to be close to 10% at pH 12.5 for the Ni(Fe)OOH film after 10 cycles, very stable OER performances and contribution from the oxygen evolution to the anodic current were found for this catalyst at every pH (Figure 2e).

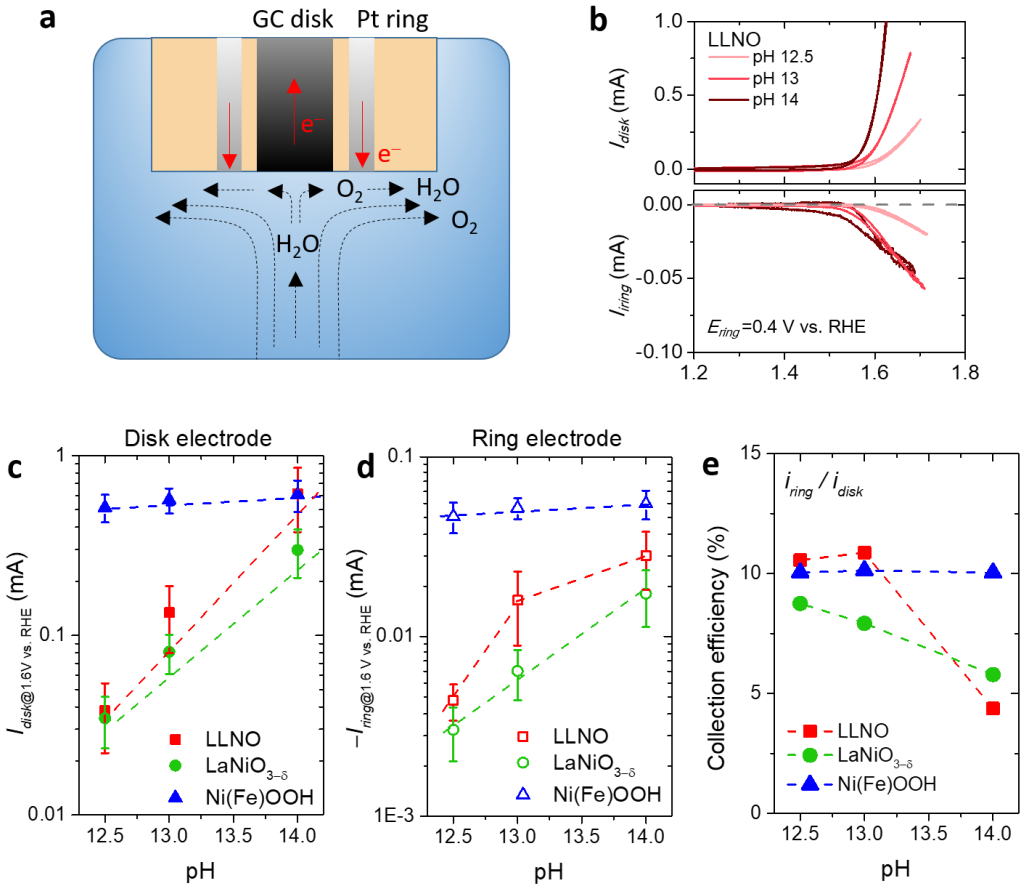

Figure 2. pH dependent activity and O_2 evolution efficiency studied by the RRDE measurement. (a) scheme for the RRDE experiment. (b) Results obtained for LLNO at pH 12.5, 13 and 14. (c) pH dependent OER activities with stabilized current measured by the disk electrode after activation for 10 cycles at a working potential of 1.6 V vs. RHE. (d) the corresponding ring current, and (e) the collection efficiency ($\eta = i_{ring}/i_{disk}$). The collection efficiency (η) of the RRDE system is estimated to be around 10 % as obtained on the electrodeposited Ni(Fe)OOH film catalyst (see methods in the Supplementary Information).

Observing that the anodic current for LLNO was found to increase with cycling at pH 13 while it was found stable for the two other Ni-based catalysts at every pH (Figure S7), we further investigated the effect of cycling on the collection efficiency as a function of pH (Figure 3). The three Ni-based model catalysts were found to demonstrate contrasted stability features when cycling at different pH. For the LLNO sample, an activation process at pH 12.5 and pH 13 during the initial 10 cycles is observed, with the collection efficiency (η) increasing from ~6% up to 12%. The low collection efficiency in the initial 1-3 cycles may be ascribed to the redox process induced by the gradual leaching of cations from the LLNO structure, whereas the high value of η obtained after activation would be a strong indication for a stable oxygen evolution current. However, when cycling LLNO at pH 14, poor oxygen evolution with a collection efficiency lower than 5% was found, suggesting that the main contribution to the anodic current originates from parasitic oxidation/corrosion phenomenon. We could further detect a continuous loss of electrochemically active surface area for LLNO at pH 14 as seen by the gradual decrease of the pseudocapacitive contribution upon cycling (Figure S9-10). For the $LaNiO_{3-\delta}$ sample, after an initial drop for the first few cycles, the ring current for oxygen detection and the collection efficiency are found relatively stable at each pH during cycling, suggesting that the rate for parasitic oxidative reaction during OER is very slow. Nevertheless, the overall collection efficiency was found to decrease with pH which suggests that the pH affects the degradation rate which gets stronger at higher pH. On the other hand, for Ni(Fe)OOH the disk current, ring current and the collection efficiency are found fairly stable upon cycling and they show no dependence on the pH.

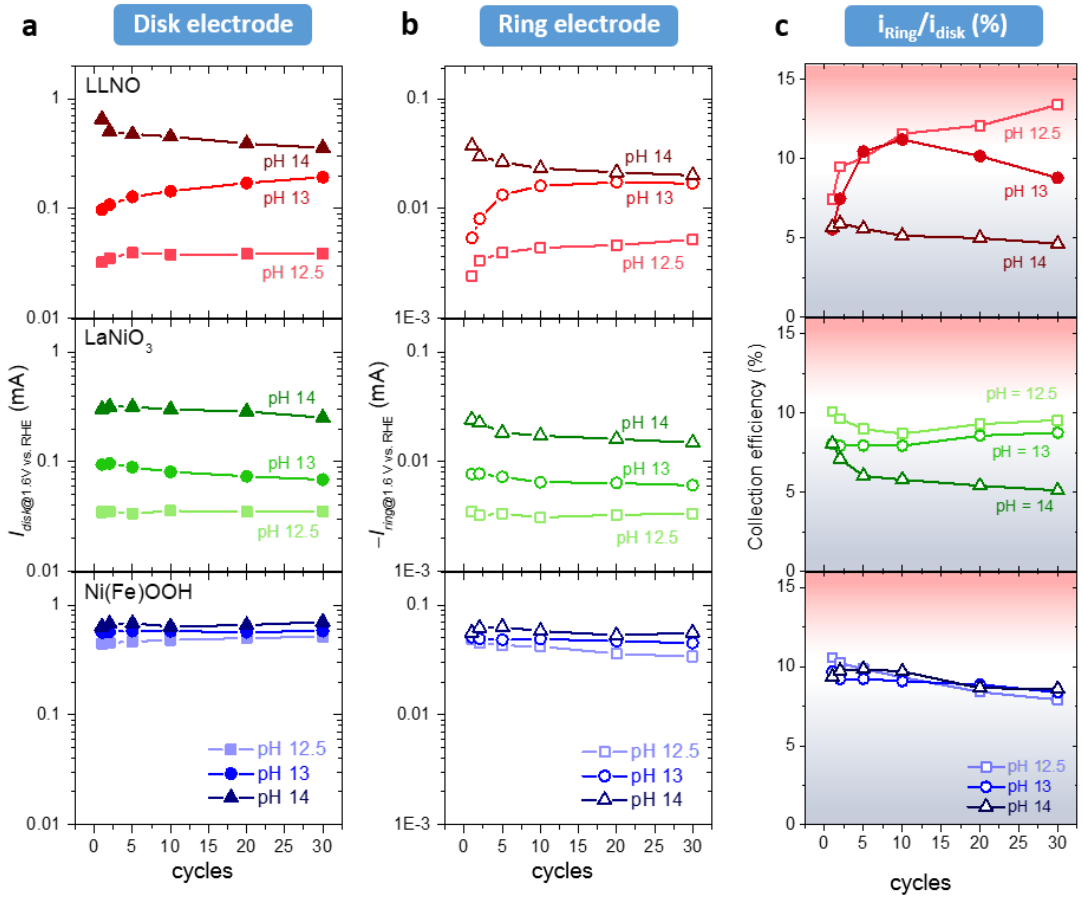

Figure 3. Electrochemical stability for the three nickel bases catalysts versus cycling and pH: LLNO, $LaNiO_{3-\delta}$, and Ni(Fe)OOH. The disk current (a), ring current (b), and the collection efficiency (c) are plotted vs. the cycling number. The low collection efficiency (η < 8%) is ascribed to the significant degradation process such as cation dissolution.

Therefore, the anodic current measured for the amorphous film arises from oxygen evolution, whereas for crystalline nickel-based oxides a non-negligible part of the current originates from a catalyst degradation process which is enhanced at high pH. We could finally show that the decreased collection efficiency found for LLNO and $LaNiO_{3-\delta}$ with pH is not arising from the use of carbon additive by showing that the collection efficiency measured for Ni(Fe)OOH is not affected by the addition of carbon (Figure S8).[36] This is consistent with the observation that the pseudocapacitive

current decreases for LLNO with cycling (Figure S9-10) while the collection efficiency is found rather constant (Figure 3c), indicative of a reduction of the electrochemically active surface area due to surface degradation while the part of the anodic current arising from the OER remains almost constant.

We further probe the degradation process occurring for these catalysts by the means of electrochemical quartz crystal microbalance (EQCM) (Figure 4). Using this weight-sensitive technique, we could conclude that the $LaNiO_{3-\delta}$ catalyst shows only a very limited mass loss during OER cycling at pH 13, with a slight drop of its mass observed at high potential. Similar observation was made for the amorphous Ni(Fe)OOH film. On the contrary, a severe mass loss is recorded for LLNO, this loss being potential-dependent and occurring above 1.5 V vs. RHE in the water oxidation region. Overall, a mass loss higher than 10 wt.% could be observed after 30 cycles, the first cycle accounting for most of this loss which gradually slows down during the subsequent cycles. Repeating these EQCM measurements at varied pH for LLNO (Figure S12), it is observed that the mass loss increases with pH. This observation is consistent with the RRDE results discussed above, and indicates that surface degradation is pH dependent for this nickel-based Ruddelsden-Popper oxide. A reversible evolution of lattice oxygen, the mechanism often proposed for the redox active compounds, would be counter-balanced by water adsorption and should not lead to any mass loss. Our results clearly show that this redox process is accompanied with drastic degradation for the LLNO catalyst.

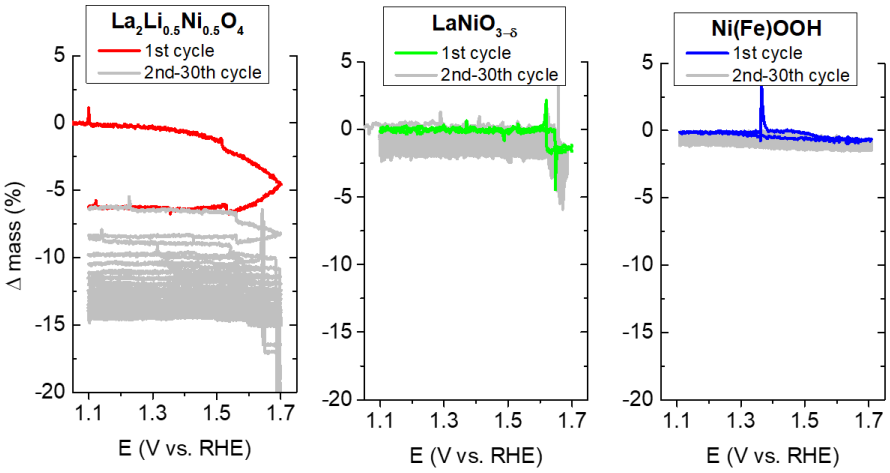

Figure 4. Comparison of the mass loss of $LaNiO_{3-\delta}$, $La_2Li_{0.5}Ni_{0.5}O_4$ and Ni(Fe) hydroxide catalysts upon cycling in KOH solution (pH = 13) recorded by electrochemical quartz crystal microbalance (EQCM).

We further studied the surface properties of the cycled LLNO and $LaNiO_{3-\delta}$ samples by HAADF-STEM and XAS at the Ni K-edge (Figure 5). A thin amorphous layer was observed on cycled LLNO samples (after 30 CV cycles), as revealed by HAADF-STEM (Figure 5a), the thickness of which grows from ≈ 2 to 6 nm when increasing the pH from 12.5 to 14. To grasp more information about the surface amorphization process, XAS at Ni K-edge was conducted in both bulk-sensitive fluorescence yield (FY) mode and surface-sensitive total electron yield (TEY) mode (Figure 5b and 5d, respectively). No significant modification of the Ni oxidation state after cycling is observed at each pH when compared to the pristine sample, unlike what could be observed for other redox active perovskites such as $Ba_{0.5}Sr_{0.5}Co_{0.8}Fe_{0.2}O_{3-\delta}$ [6, 37] The corresponding EXAFS spectra also confirmed that the atomic local environment on the surface of this oxide is maintained upon cycling, with the apparition of a new feature at around 2 Å in reduced distances which would correspond to an edge-shared octahedra coordination growing with pH. EDX analysis was then conducted to provide information about the chemical compositions of the

amorphous film (Figure S13). When compared to the bulk crystals, the amorphous layer shows similar elemental distributions including Ni, La, and O. Recrystallization process of the surface is observed under the electron beam (Figure S13), with only a loss of long range order possibly due to atomic defects (vacancies) formed upon cycling. This observation indicates that not only Li is leached out during cycling, but that La and Ni cations are also continuously lost on the surface leading to a drastic loss of mass as shown by EQCM. Hence, these results show that the amorphous thin layer formed on the LLNO surface mostly originates from the redox activity of the surface, suggesting that the edge-shared octahedra motifs observed by EXAFS grow farther from the surface of the particles. Nevertheless, this result cannot explain the loss of more than 10% in mass of catalyst as recorded by EQCM (Figure 4a). Bearing in mind that the solubility of nickel in alkaline conditions is rather small, we hypothesize that clusters of nickel hydroxides could be formed in solution away from the electrode and do not deposit onto the surface of crystalline LLNO.

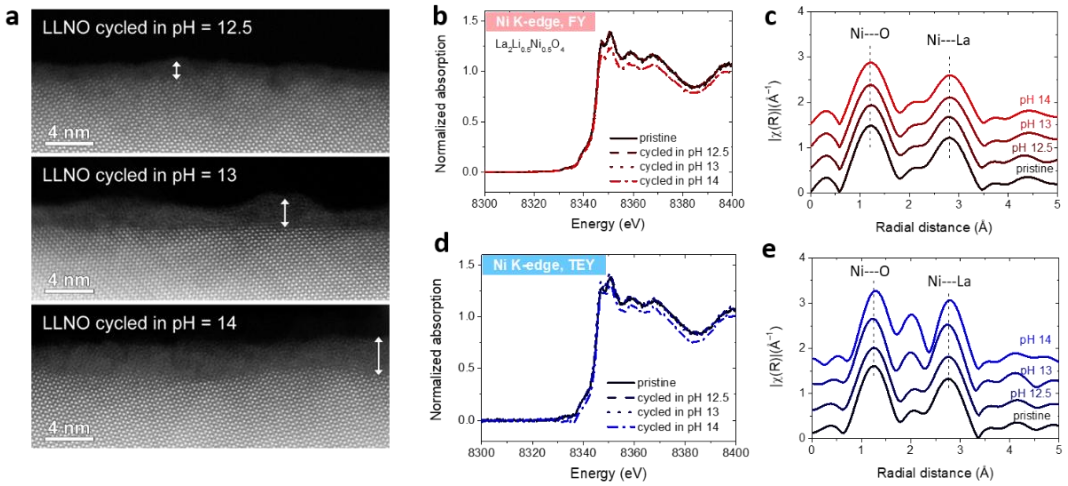

Figure 5. Surface deconstruction of $La_2Li_{0.5}Ni_{0.5}O_4$ catalyst. (a) HAADF-STEM images of cycled LLNO catalysts in KOH solutions at different pH. (b-e) Ni K-edge X-ray absorption spectra and the corresponding EXAFS oscillations recorded for LLNO after cycling in KOH solutions at different pH. (b) and (c) are recorded in the bulk-sensitive fluorescence mode (FY), (d) and (e) are recorded in surface-sensitive total electron

yield (TEY) mode.

As suggested in this work, the electrochemical activity and stability of oxide catalysts are related to their crystal and electronic structures but also to the pH of the supporting electrolyte. Using LLNO as a model compound, we show that pH dependence for the anodic current measured with crystalline compounds can be associated with severe surface degradation and lower oxygen evolution efficiencies, unlike for amorphous catalysts. Combining post mortem analysis, we could explain this phenomenon in terms of surface instability and degradation related to cations leaching at high potential. Therefore, we believe that in order to accurately evaluate the intrinsic OER activities of highly active oxide catalysts which may involve the redox activity of lattice oxygen, it is essential to decouple the contributions of the water oxidation and the oxygen evolution from the degradation processes associated with catalyst degradation under anodic current. Toward this perspective, the use of RRDE experiments appears as a promising strategy for accurately assessing the true oxygen evolution contribution to the anodic current.[31] In addition to RRDE, more efforts should be devoted to developing proper characterizations for online detection of gas evolution[38], mass dissolution[39], and intermediates formation by surface-enhanced Raman spectroscopy[40] to provide more in-depth information about the complex surface dynamics involved during the OER. We believe that this work will set up future strategies to assess the real performances of potential OER catalysts and we can foresee that catalyst structuration, which has been critical for developing advanced oxygen reduction reaction (ORR) catalysts,[41] will become even more important for designing stable and active OER catalysts.

Acknowledgements

C.Y., J.-M.T. and A.G. acknowledge funding from the European Research Council (ERC) (FP/2014)/ERC Grant-Project 670116-ARPEMA. A.G. acknowledges financial support from the ANR MIDWAY (Project ID: ANR-17-CE05-0008). We acknowledge Diamond Light Source for time awarded to the Energy Materials BAG on Beamline B18, under Proposal sp12559.

Supporting Information

The Supporting Information is available free of charge on the ACS

Publications website at DOI: XXXX

Experiment description, more physical characterizations and electrochemical data analyses are presented in the supporting information.

References

(1) Hunter, B. M.; Gray, H. B.; Muller, A. M., Earth-Abundant Heterogeneous Water Oxidation Catalysts. *Chem. Rev.* **2016**., 116 (22), 14120-14136.

(2) Dau, H.; Limberg, C.; Reier, T.; Risch, M.; Roggan, S.; Strasser, P., The Mechanism of Water Oxidation: From Electrolysis via Homogeneous to Biological Catalysis. *ChemCatChem* **2010,** *2* (7), 724-761.

(3) Grimaud, A.; May, K. J.; Carlton, C. E.; Lee, Y. L.; Risch, M.; Hong, W. T.; Zhou, J.; Shao-Horn, Y., Double Perovskites as a Family of Highly Active Catalysts for Oxygen Evolution in Alkaline Solution. *Nat. Commun.* **2013,** *4*, 2439.

(4) Mefford, J. T.; Rong, X.; Abakumov, A. M.; Hardin, W. G.; Dai, S.; Kolpak, A. M.; Johnston, K. P.; Stevenson, K. J., Water Electrolysis on $La_{1-x}Sr_xCoO_{3-\delta}$ Perovskite Electrocatalysts. *Nat. Commun.* **2016,** *7*, 11053.

(5) Yagi, S.; Yamada, I.; Tsukasaki, H.; Seno, A.; Murakami, M.; Fujii, H.; Chen, H.; Umezawa, N.; Abe, H.; Nishiyama, N.; Mori, S., Covalency-reinforced Oxygen Evolution Reaction Catalyst. *Nat. Commun.* **2015,** *6*, 8249.

(6) Fabbri, E.; Nachtegaal, M.; Binninger, T.; Cheng, X.; Kim, B.-J.; Durst, J.; Bozza, F.; Graule, T.; Schäublin, R. *et al.*, Dynamic Surface Self-reconstruction is the Key of Highly Active Perovskite Nano-electrocatalysts for Water Splitting. *Nat. Mater.* **2017,** *16* (9), 925-931.

(7) Macounova, K.; Makarova, M.; Krtil, P., Oxygen Evolution on Nanocrystalline

RuO_2 and $Ru_{0.9}Ni_{0.1}O_{2-\delta}$ Electrodes – DEMS Approach to Reaction Mechanism Determination. *Electrochem. Commun.* **2009,** *11* (10), 1865-1868.

(8) Diaz-Morales, O.; Calle-Vallejo, F.; de Munck, C.; Koper, M. T. M., Electrochemical Water Splitting by Gold: Evidence for an Oxide Decomposition Mechanism. *Chem. Sci.* **2013,** *4* (6), 2334-2343.

(9) Doornkamp, C.; Ponec, V., The Universal Character of the Mars and Van Krevelen Mechanism. *J. Mol. Catal. A: Chem.* **2000,** *162* (1-2), 19-32.

(10) Grimaud, A.; Demortiere, A.; Saubanere, M.; Dachraoui, W.; Duchamp, M.; Doublet, M.-L.; Tarascon, J.-M., Activation of Surface Oxygen Sites on an Iridium-Based Model Catalyst for the Oxygen Evolution Reaction. *Nat. Energy* **2016,** *2* (1), 16189.

(11) Costentin, C.; Nocera, D. G., Self-healing Catalysis in Water. *Proc. Natl. Acad. Sci. U.S.A.* **2017,** *114* (51), 13380-13384.

(12) Chang, S. H.; Danilovic, N.; Chang, K.-C.; Subbaraman, R.; Paulikas, A. P.; Fong, D. D.; Highland, M. J.; Baldo, P. M.; Stamenkovic, V. R.; Freeland, J. W. *et al.*, Functional Links Between Stability and Reactivity of Strontium Ruthenate Single Crystals during Oxygen Evolution. *Nat. Commun.* **2014,** *5*. 4191

(13) Kasian, O.; Grote, J.-P.; Geiger, S.; Cherevko, S.; Mayrhofer, K. J. J., The Common Intermediates of Oxygen Evolution and Dissolution Reactions during Water Electrolysis on Iridium. *Angew. Chem., Int. Ed. Engl.* **2018**, *57* (9), 2488-2491.

(14) Giordano, L.; Han, B.; Risch, M.; Hong, W. T.; Rao, R. R.; Stoerzinger, K. A.; Shao-Horn, Y., pH Dependence of OER Activity of Oxides: Current and Future Perspectives. *Catalysis Today* **2016,** *262*, 2-10.

(15) Grimaud, A.; Hong, W. T.; Shao-Horn, Y.; Tarascon, J. M., Anionic Redox Processes for Electrochemical Devices. *Nat. Mater.* **2016,** *15* (2), 121-126.

(16) Yang, C.; Laberty-Robert, C.; Batuk, D.; Cibin, G.; Chadwick, A. V.; Pimenta, V.; Yin, W.; Zhang, L.; Tarascon, J. M.; Grimaud, A., Phosphate Ion Functionalization of Perovskite Surfaces for Enhanced Oxygen Evolution Reaction. *J. Phys. Chem. Lett.* **2017,** *8* (15), 3466-3472.

(17) Trześniewski, B. J.; Diaz-Morales, O.; Vermaas, D. A.; Longo, A.; Bras, W.; Koper, M. T. M.; Smith, W. A., *In Situ* Observation of Active Oxygen Species in Fe-Containing Ni-Based Oxygen Evolution Catalysts: The Effect of pH on Electrochemical Activity. *J. Am. Chem. Soc.* **2015,** *137* (48), 15112-15121.

(18) Hong, W. T.; Stoerzinger, K. A.; Lee, Y.-L.; Giordano, L.; Grimaud, A.; Johnson, A. M.; Hwang, J.; Crumlin, E. J.; Yang, W.; Shao-Horn, Y., Charge-transfer-energy-dependent Oxygen Evolution Reaction Mechanisms for Perovskite Oxides. *Energy & Environmental Science* **2017,** *10* (10), 2190-2200.

(19) Yang, C.; Fontaine, O.; Tarascon, J. M.; Grimaud, A., Chemical Recognition of

Active Oxygen Species on the Surface of Oxygen Evolution Reaction Electrocatalysts. *Angew. Chem. Int. Ed. Engl.* **2017,** *56* (30), 8652-8656.

(20) Spoeri, C.; Kwan, J. T. H.; Bonakdarpour, A.; Wilkinson, D.; Strasser, P., The Stability Challenges of Oxygen Evolving Electrocatalysts: Towards a Common Fundamental Understanding and Mitigation of Catalyst Degradation. *Angew. Chem. Int. Ed. Engl.* **2017**, *56*, 5994.

(21) Rong, X.; Parolin, J.; Kolpak, A. M., A Fundamental Relationship between Reaction Mechanism and Stability in Metal Oxide Catalysts for Oxygen Evolution. *ACS Catalysis* **2016,** *6* (2), 1153-1158.

(22) Han, B.; Stoerzinger, Kelsey A.; Tileli, V.; Gamalski, Andrew D.; Stach, Eric A.; Shao-Horn, Y., Nanoscale Structural Oscillations in Perovskite Oxides Induced by Oxygen Evolution. *Nat. Mater.* **2016,** *16* (1), 121-126.

(23) Chang, S. H.; Connell, J. G.; Danilovic, N.; Subbaraman, R.; Chang, K.-C.; Stamenkovic, V. R.; Markovic, N. M., Activity–Stability Relationship in the Surface Electrochemistry of the Oxygen Evolution Reaction. *Faraday Discuss.* **2014,** *176*, 125-133.

(24) Kanan, M. W.; Nocera, D. G., In situ Formation of an Oxygen-evolving Catalyst in Neutral Water Containing Phosphate and Co^{2+}. *Science* **2008,** *321* (5892), 1072-1075.

(25) Kanan, M. W.; Surendranath, Y.; Nocera, D. G., Cobalt–phosphate Oxygen-evolving Compound. *Chem. Soc. Rev.* **2009,** *38* (1), 109-114.

(26) Trotochaud, L.; Young, S. L.; Ranney, J. K.; Boettcher, S. W., Nickel–Iron Oxyhydroxide Oxygen-Evolution Electrocatalysts: The Role of Intentional and Incidental Iron Incorporation. *J. Am. Chem. Soc.* **2014,** *136* (18), 6744-6753.

(27) Man, I. C.; Su, H.-Y.; Calle-Vallejo, F.; Hansen, H. A.; Martínez, J. I.; Inoglu, N. G.; Kitchin, J.; Jaramillo, T. F.; Nørskov, J. K.; Rossmeisl, J., Universality in Oxygen Evolution Electrocatalysis on Oxide Surfaces. *ChemCatChem* **2011,** *3* (7), 1159-1165.

(28) May, K. J.; Carlton, C. E.; Stoerzinger, K. A.; Risch, M.; Suntivich, J.; Lee, Y.-L.; Grimaud, A.; Shao-Horn, Y., Influence of Oxygen Evolution during Water Oxidation on the Surface of Perovskite Oxide Catalysts. *J. Phys. Chem. Lett.* **2012,** *3* (22), 3264-3270.

(29) Friebel, D.; Louie, M. W.; Bajdich, M.; Sanwald, K. E.; Cai, Y.; Wise, A. M.; Cheng, M.-J.; Sokaras, D.; Weng, T.-C.; Alonso-Mori, R. *et al.*, Identification of Highly Active Fe Sites in (Ni,Fe)OOH for Electrocatalytic Water Splitting. *J. Am. Chem. Soc.* **2015,** *137* (3), 1305-1313.

(30) Köhler, L.; Ebrahimizadeh Abrishami, M.; Roddatis, V.; Geppert, J.; Risch, M., Mechanistic Parameters of Electrocatalytic Water Oxidation on $LiMn_2O_4$ in

Comparison to Natural Photosynthesis. *ChemSusChem* **2017,** *10* (22), 4479-4490.

(31) Filimonenkov, I. S.; Istomin, S. Y.; Antipov, E. V.; Tsirlina, G. A.; Savinova, E. R., Rotating Ring-Disk Electrode as a Quantitative Tool for the Investigation of the Oxygen Evolution Reaction. *Electrochimica Acta* **2018,** *286*, 304-312.

(32) Abou-Warda, S.; Pietzuch, W.; Berghöfer, G.; Kesper, U.; Massa, W.; Reinen, D., Ordered K_2NiF_4 Structure of the Solids $La_2Li_{1/2}M_{1/2}O_4$ (M(III)=Co, Ni, Cu) and the Bonding Properties of the MO_6 Polyhedra in Various Compounds of This Type. *Journal of Solid State Chemistry* **1998,** *138* (1), 18-31.

(33) Goerlin, M.; Chernev, P.; Ferreira de Araujo, J.; Reier, T.; Dresp, S.; Paul, B.; Kraehnert, R.; Dau, H.; Strasser, P., Oxygen Evolution Reaction Dynamics, Faradaic Charge Efficiency, and the Active Metal Redox States of Ni-Fe Oxide Water Splitting Electrocatalysts. *J. Am. Chem. Soc.* **2016,** *138* (17), 5603–5614.

(34) Goldsmith, Z. K.; Harshan, A. K.; Gerken, J. B.; Vörös, M.; Galli, G.; Stahl, S. S.; Hammes-Schiffer, S., Characterization of NiFe Oxyhydroxide Electrocatalysts by Integrated Electronic Structure Calculations and Spectroelectrochemistry. *Proc. Natl. Acad. Sci. U.S.A.* **2017,** *114* (12), 3050-3055.

(35) Zhou, W.; Sunarso, J., Enhancing Bi-functional Electrocatalytic Activity of Perovskite by Temperature Shock: A Case Study of $LaNiO_{3-\delta}$. *J. Phys. Chem. Lett.* **2013,** *4* (17), 2982-2988.

(36) Wang, W.; Luo, J.; Chen, S., Carbon Oxidation Reactions Could Misguide the Evaluation of Carbon Black-based Oxygen-evolution Electrocatalysts. *Chem. Commun.* **2017,** *53* (84), 11556-11559.

(37) Risch, M.; Grimaud, A.; May, K. J.; Stoerzinger, K. A.; Chen, T. J.; Mansour, A. N.; Shao-Horn, Y., Structural Changes of Cobalt-Based Perovskites upon Water Oxidation Investigated by EXAFS. *J. Phys. Chem. C* **2013,** *117* (17), 8628-8635.

(38) Grimaud, A.; Diaz-Morales, O.; Han, B.; Hong, W. T.; Lee, Y. L.; Giordano, L.; Stoerzinger, K. A.; Koper, M. T. M.; Shao-Horn, Y., Activating Lattice Oxygen Redox Reactions in Metal Oxides to Catalyse Oxygen Evolution. *Nat. Chem.* **2017,** *9* (5), 457-465.

(39) Schmies, H.; Bergmann, A.; Drnec, J.; Wang, G.; Teschner, D.; Kühl, S.; Sandbeck, D. J. S.; Cherevko, S.; Gocyla, M.; Shviro, M. *et al.*, Unravelling Degradation Pathways of Oxide-Supported Pt Fuel Cell Nanocatalysts under In Situ Operating Conditions. *Adv. Energy Mater.* **2018,** *8* (4), 1701663.

(40) Yeo, B. S.; Klaus, S. L.; Ross, P. N.; Mathies, R. A.; Bell, A. T., Identification of Hydroperoxy Species as Reaction Intermediates in the Electrochemical Evolution of Oxygen on Gold. *ChemPhysChem* **2010**, *11*, 1854-1857.

(41) Kim, Y.-T.; Lopes, P. P.; Park, S.-A.; Lee, A. Y.; Lim, J.; Lee, H.; Back, S.; Jung, Y.;

Danilovic, N.; Stamenkovic, V.; Erlebacher, J.; Snyder, J.; Markovic, N. M., Balancing Activity, Stability and Conductivity of Nanoporous Core-shell Iridium/Iridium Oxide Oxygen Evolution Catalysts. *Nat. Commun.* **2017**, 8 (1), 1449.